HHS Public Access

Author manuscript

Phys Med Biol. Author manuscript; available in PMC 2020 June 25.

Published in final edited form as:

Phys Med Biol. ; 65(10): 105012. doi:10.1088/1361-6560/ab8106.

Quantifying vascular invasion in pancreatic cancer - a contrast CT based method for surgical resectability evaluation

Yi Lao, Ph.D.[1], **John David, M.D.**[2], **Zhaoyang Fan, Ph.D.**[3], **Shelly Bian, M.D.**[4], **Almon Shiu, Ph.D.**[4], **Eric L Chang, M.D.**[4], **Ke Sheng, Ph.D.**[1], **Wensha Yang, Ph.D.**[4,*], **Richard Tuli, M.D., Ph.D**[5,*]

[1]Department of Radiation Oncology, University of California-Los Angeles, Los Angeles, USA

[2]Department of Radiation Oncology, Cedars-Sinai Medical Center, Los Angeles, USA

[3]Department of Biomedical Sciences, Cedars-Sinai Medical Center, Los Angeles, USA

[4]Department of Radiation Oncology, University of Southern California, Los Angeles, USA

[5]Department of Radiation Oncology, Memorial Sloan Kettering Cancer Center, New York, USA

Abstract

Pancreatic cancer (PC) is one of the most lethal cancers, with frequent local therapy resistance and dismal 5-year survival rate. To date, surgical resection remains to be the only treatment option offering potential cure. Unfortunately, at diagnosis, the majority of patients demonstrate varying levels of vascular infiltration, which can contraindicate surgical resection. Patients unsuitable for immediate resection are further divided into locally advanced (LA) and borderline resectable (BR), with different treatment goals and therapeutic designs. Accurate definition of resectability is thus critical for PC patients, yet the existing methods to determine resectability rely on descriptive abutment to surrounding vessels rather than quantitative geometric characterization. Here, we aim to introduce a novel intra-subject object-space support-vector-machine (OsSVM) method to quantitatively characterize the degree of vascular involvement -- the main factor determining the PC resectability. Intra-subject OsSVMs were applied on 107 contrast CT scans (56 LA, BR and 26 resectable (RE) PC cases) for optimized tumor-vessel separations. Nine metrics derived from OsSVM margins were calculated as indicators of the overall vascular infiltration. The combined sets of matrics selected by the elastic net yielded high classification capability between LA and BR (AUC=0.95), as well as BR and RE (AUC=0.98). The proposed OsSVM method may provide an improved quantitative imaging guideline to refine the PC resectability grading system.

Keywords

Computer-Aided Diagnosis; Quantitative Resectability; SVM; Contrast-CT; Pancreatic Cancer

[*]co-corresponding author: 323-865-3089 (o), Wensha.Yang@med.usc.edu, Rtuli01@gmail.com.

The authors declare no conflicts of interest.

1 Introduction

Pancreatic cancer (PC) is one of the most malignant cancers, with a collective median survival of 4–6 months and a 5-year survival rate as low as 5% [1, 2]. Currently, surgical resection remains to be the only potentially curable treatment, which increases the 5-year survival rate to 12–20%, compared to <1% for unresectable cases [3]. However, at the time of diagnosis, only an estimated 10% - 20% of patients present with resectable disease. The majority of patients demonstrate varying levels of vascular infiltration, which can contraindicate surgical resection. Patients with tumor vasculature infiltration are further classified into borderline resectable (BR) and locally advanced (LA) PC, which are subject to different treatment goals and therapeutical regimens. As a result, differentiating patients with surgical potential from those with unresectable diseases is of paramount importance in patient management. However, there is a scarcity of standardized criteria for defining resectability.

The ambivalence in the existing clinical definition of resectability is in part attributed to the lack of consensus over multiple radiologic grading systems. The criteria of resectability have been evolving with the advances of surgical techniques. Tumors once considered locally advanced may now have surgical potential. For instance, any degree of involvement from superior mesenteric vein/ portal vein (SMV/PV) would have precluded the tumor from resection using criteria from decades ago [4], while the newer National Comprehensive Cancer Network (NCCN) and Alliance guidelines consider SMV/PV involvement up to 180° for surgical resection [5, 6]. Moreover, since the concept of resectability implies a subjective consensus between a specific surgeon and a radiologist, substantial inter-institutional variability exists [5].

The coarsely descriptive guideline in current radiologic grading systems is another barrier to implement standardized resectability definition [7, 8]. Current PC resectability definition categorized abutment of vessels derived from contrast-enhanced computerized tomography (CT). Targeting at only a few major vessels, such as PV, SMV, SMA (superior mesenteric artery), the crude criteria are unable to assess the overall vascular involvement and the wide spectrum of patients from deemed unresectable to resectable. As illustrated in Figure 1, while current criteria based on axial views (top row) have roughly divided the left 5 subjects as 3 LA and 2 BR, 3D renderings (middle row) show different levels of vascular involvement within each diagnostic group. In addition, the current classification of the vessel abutment (e.g.<180°, ≥180°) complicates the interpretation of patients falling into the categorical boundaries, thus is prone to inter-observer variabilities. Furthermore, for response assessment, there are large gaps between resectable (RE), BR and LA using current criteria, resulting in insensitive detection of tumor partial responses (i.e. tumors partially regressed, albeit failed to be downgraded below the BR/RE threshold). Therefore, to develop an objective grading system of resectability that is sensitive to the subtle variation of disease status, a quantitative measurement of vascular involvement is clearly needed.

In this study, we introduce a novel organ-space support vector machine (OsSVM) based method for PC resectability evaluation on contrast-CT. Our aim is two-fold: first, to quantitatively characterize the tumor-vessel relationship using intra-subject OsSVM derived

metrics; second, to validate the feasibility of using the derived metrics to classify PC groups with varying resectability (LA, BR, and RE).

2 Methods

2.1 Subjects and Data

Under Institutional Review Board (IRB) approval, 92 PC patients aged 31–90 years (mean: 65.4, std:11.6) were retrospectively solicited from our institutional database between 2011 to 2018. The CT imaging analysis was carried out in accordance with the minimal risk policy defined by the IRB. The selection criteria are as follows: 1) having undergone diagnostic contrast CT scan at our facility; 2) clinical diagnosis of resectability (LA, BR or RE). 3) RE patients underwent margin-negative resection. Fifteen of the 92 patients with the initially unresectable disease were downstaged to RE after neoadjuvant treatment. They were then treated as independent subjects in this analysis, increasing the total of PC cases to 107 (56 LA, 25 BR, and 26 RE). Each patient underwent an abdominal contrast CT scan with 100 cc iodixanol, 350mg I/ml contrast injection. Multiple CT scanners were used including Optima 580, HiSpeed NX/i, LightSpeed VCT (General Electric HealthCare, Massachusetts, U.S.); and Gemini (Philips Healthcare, Amsterdam, Netherlands). Hepatic phase scans were obtained approximately 60 seconds after the contrast agent injection. Most of the CT images have spatial resolution of 1.26mm × 1.26mm × 2.5mm, with pixel spacing ranging from 1–1.26 mm and slice thickness ranging from 2.5–5 mm. Quality assurance was routinely performed on all CT scanners to maintain consistent inter-scanner calibration through time.

2.2 Data preprocessing

The processing pipeline is illustrated in Figure 2. On the contrast CT, tumor boundaries and surrounding vessels were manually delineated by a radiation oncologist (>5 years of experience). Vessels were segmented mainly on axial slices spanning the tumor superior-inferior extension, with 10 mm margin on both ends. The intra-rater reliability (intersection over union) score was 0.89 for tumor and 0.93 for vessels, among four participants at two different time points spanning eight weeks.

Segmentation of tumors and surrounding vessels were converted to the individual-wise volume of interest (VOI). To reduce the inter-subject variation, VOIs were first resampled to the same dimension ($1\times1\times1 mm$) and then transformed to the corresponding center of mass. A bounding box extending $10 mm$ outside the tumor boundaries was further applied to include vessels that adjacent to the tumor. The harmonized VOIs were used to build statistical tumor-vessel relationship models in the following steps.

2.3 Hyperplane and critical points

A radial basis function (RBF) kernel SVM classifier [9, 10] was used to define the intricate tumor-vessel relationship by separating the two structures according to their anatomical locations. Specifically, with points x_i in the VOI and the corresponding class y_i (1 for tumor, −1 for the vessel), we aim to find the decision surface that separates the two structures with the maximized margin. The decision surface is termed a hyperplane in SVM. To find the

optimal hyperplane, it is computationally efficient to solve for the Lagrangian dual formation with the constraints such that:

$$\begin{aligned} &max L_D(\alpha_i) \sum_i \alpha_i - \frac{1}{2} \sum_i \sum_j \alpha_i \cdot \alpha_j \cdot y_i \cdot y_j \cdot K(x_i \cdot x_j) \\ &s.t. \\ &\sum_i y_i \alpha_i = 0 \\ &0 \le \alpha_i \le C. \end{aligned} \tag{1}$$

where K is an RBF kernel (with kernel scale γ) that transforms the linearly inseparable data into a higher dimensional space, C is a box constraint which trades off the fit of solutions with the simplicity of the hyperplane. The non-zero Lagrange multipliers (α) from the optimizing process play a critical role in determining the location of the hyperplane and correspond to the support vectors.

Different from traditional SVM analysis that seeks a single model for the whole patient cohort, here we aim to build a patient-specific model and then compare the levels of misclassification among different PC groups. Same hyper-parameter settings were used for individual patient models to afford fair inter-subject comparisons. Using randomly selected 10 RE cases as a test set, $\gamma = 4$ and C=10 were set to achieve a reasonable runtime and low misclassification rate in the RE cases (Figure 3).

2.4 Margins of critical points

Resectability is analogous to the separability between the class *tumor* and the class *vessel*, which can be determined by the margins of the critical points (support vectors). The classification margin, a confidence measure of the separation, is defined as:

$$m_i = 2 y_i f(x_i) \tag{2}$$

where x_i is an observation, $y_i \in \{-1, 1\}$ is the corresponding true label, and $f(x_i)$ is the predicted score from the above SVM model. A larger m value represents a higher classification confidence of the observation. The magnitude and distribution of m from the critical points corresponding to the class *vessel* characterize the extent of vascular invasion. In this study, several margin-derived metrics were developed/adopted to quantify misclassification of each individual OsSVM model. The margin-derived metrics are described as follows.

First, deeply penetrating vessel points, or points with lower classification confidence, impact the resectability more than the less invasive points. Thus, P_{vi} was defined to heavily penalize the deeply embedded vessel points in the estimation of overall vascular invasion:

$$P_{vi} = \sum_i \frac{1}{e^{(m_i - 2)}} \tag{3}$$

It would also be of clinical interest to determine the maximum vascular penetration level so that vessels with a small portion deeply invaded by the tumor can be differentiated from the

vessels with a large portion with shallow tumor infiltration, despite their similar P_{vi} values. Given the anatomies of the pancreatic tumors and major surrounding vessels, separation hyperplanes were mainly oriented in the inferior-superior direction (Figure. 2 (b)), or Z direction. The maximum penetration was calculated as:

$$P_{max} = \max_{z_u \in z} \{ \sum_{\{x_i \in SV_v : x_{iz} = z_u\}} m_i \} \quad (4)$$

In addition to P_{vi} and P_{max}, the average and variance of critical point margins (P_{mean} *and* P_{var}) were also used as two intuitive indicators of the margin distribution. In addition, since the histogram is also effective in interpreting data distribution, such as the asymmetry and outliers [11], five commonly used histogram-based metrics were included in the analysis: mean (H_{mean}), variance (H_{var}), skewness (H_{skew}), kurtosis (H_{kurt}), and energy (H_{ener})). Note that the referred histograms were calculated based on the distribution of margins, which are different from image intensity based histograms commonly used in radiomic features [12, 13].

2.5 Statistical analysis

Between-group student *t*-tests were first employed for each metric independently to evaluate their corresponding classification capacity differentiating LA and BR. The classification power was further tested using logistic regression followed by receiver operating characteristic (ROC) analyses.

To test if a combination of multiple metrics would further increase classification power, regularized logistic regression via the elastic net (EN) was used to narrow down a selection of features [14]. Specifically, using:

$$\underset{\beta}{\operatorname{argmin}} \{ \frac{1}{N} \sum_{i=1}^{N} L(\beta, X, Y) - \lambda [(1-\alpha) \frac{\|\beta\|_2{}^2}{2} + \alpha \|\beta\|_1] \} \quad (5)$$

where X is the input feature set, Y is the corresponding group label set (0 for LA, 1 for BR), β is the regression coefficient, and λ is a regularization parameter. The size of β is penalized by EN based on a weighting of the L^1- and L^2-norms, where L^1-norm encourages feature sparsity and L^2-norm encourages feature grouping. The weighting coefficient α is selected as 0.5. The model was validated through 8-fold cross-validation with one standard deviation. The classification power of metrics selected by EN was then evaluated by ROC analysis.

The same analyses were also applied to discriminate RE from BR, as well as RE from all unresectable cases (UnRE, LA + BR).

3 Results

3.1 Metric distributions and Group comparisons

Figure. 4 shows the box plots of all 9 OsSVM derived metrics. The mean P_{vi}, P_{max}, P_{var}, H_{var}, and H_{skew} of LA, BR, and RE decrease following the order of tumor involvement. On the other hand, the mean P_{mean}, H_{mean}, H_{kurt}, and H_{ener} showed the opposite trends,

indicating increasing confidence of tumor-vessel separation from LA to RE. The correlation between one of OsSVM derived metrics and resectability is shown in Figure. 1, where P_{vi} decreases monotonously with increasing resectability. The corresponding pair-wise group comparisons are displayed in Table. 1. All metrics significantly ($p<0.05$) differentiate between LA and BR, BR and RE, as well as UnRE and RE.

3.2 Univariate and multivariate regressions

ROC analyses of the OsSVM derived metrics are shown in Table. 2 and Figure. 5. Not surprisingly, by penalizing the penetrating vascular points, P_{max} and P_{vi} were the 2 most sensitive classifiers for LA and BR (Figure. 5 (a)), yielding AUCs of 0.91 and 0.89, respectively. Based on 8-fold cross-validation, five of the nine metrics (P_{max}, P_{vi}, P_{mean}, $H_{skew,}$ and H_{kurt}) were selected by the elastic net as significant features (Table. 2). The classification accuracy combining the five features outperformed any single feature, achieving AUC of 0.95.

For the classification of BR and RE, all metrics except P_{vi} yield AUCs greater than 0.96, indicating a clear differentiation of tumor vessel infiltration between the two groups using OsSVM model. Four metrics (P_{max}, P_{var}, P_{mean}, and H_{ener}) were selected by the elastic net as significant features. The combined metrics further improved the AUC to 0.98. By merging LA and BR to be a single UnRE group, consistently better AUC performance than the classification of BR and RE was observed likely due to larger sample size. In the merged case to differentiate RE from UnRE, six metrics (P_{max}, P_{vi}, P_{var}, P_{mean}, H_{ener}, and H_{var}) were selected by the elastic net resulting nearly perfect AUC.

4 Discussion

Defining resectability is essentially a problem of interpreting the relative spatial relationships of two image objects: the tumor and the vessels. Among the existing tools, force histograms (*F*-histograms) are state-of-the-art descriptors to interpret directional relations, such as ‘among’, ‘between’, and ‘surround’ [15, 16]. The fuzzy model has been further developed to quantify the semantic directional description so that the degree to which a target object is in a certain direction with respect to a reference object can be evaluated [17, 18]. While playing a vital role in interpreting images with simple shapes, F-histograms or fuzzy models inadequately integrate the topological and distance information of objects in spatial relation reasoning, thus cannot model complicated spatial relationships in medical images, especially with the presence of blood vessels.

For complex spatial configurations, Clément et. al characterized the degree of imbrication in 2D retinal images using an advanced circular histogram algorithm [19]. However, the imbrication metric may not accurately describe PC resectability because the spacing between the image objects was not integrated into the calculation. Toesca DA et. al provided a 0–10 score criterion based on the maximum circumferential degree and length of solid tumor contact in CT images [20]. With a decision tree derived cut-off in 294 patients, this finer scoring system achieved an accuracy of 97% in R0 resection prediction. However, the semi-quantitative criterion still relied on unidimensional measurements on a limited of major peripancreatic vessels, and thus lack overall estimation of the whole perivascular

involvement. To extract more insights over the whole 3D tumor volume, Van der Putten et. al had tried to use radiomic features, drawn from intensities and spatial arrangement of voxels, to predict resectability. Specifically, from 90 radiomic features, he used the Relieff feature selection to narrow down a set of 9 features in 50 patients and achieved a sensitivity of 93% and a specificity of 67% in resectable versus unresectable classification [21]. While providing additional insights about tumor heterogeneity, the application of radiomics in PC resectability is limited by the unclear interpretability of the radiomic features and the imbalance between number of features and sample size [22].

We took a different approach in this study. Mimicking the goal of surgical resection, we used OsSVM classifiers to create a hyperplane that maximally separates the tumor and vessels. The resultant misclassification correlates to the level of vascular infiltration. The margin calculation based on critical points is consistent with the actual clinical condition that only the portion of vessels adjacent to the resection margin matters. The efficacy of the OsSVM model is highlighted in Figure 1, where the inter-subject differences spanning the wide spectrum from LA to RE is quantitatively correlated to one of the OsSVM metrics. As an example, two cases presenting similar appearance in the axial slices (LA3 and BR1) could have been miss-classified based on the current NCCN guidelines but they were continuously placed on the resectability spectrum based on the P_{vi} values. Therefore, our method is innovative in quantitatively describing the complex tumor/vessel relationships for finer categorization of PC resectability.

Our current work has two limitations. First, the OsSVM model was built based on manual segmentation. While careful quality control was implemented, delineation variabilities cannot be completely avoided. The uncertainties may be amplified by the fact that multiple CT scanners/protocols were used in this retrospective study. However, this effect is expected to be small due to consistent image quality calibration procedures implemented at our institution. With the advances of deep learning, automated contouring algorithms emerged to maintain high segmentation accuracy against multi-institutional, multi-protocol dataset [23]. Therefore, automated segmentation techniques shall be integrated into our future pipeline to increase the robustness against segmentation variability. Second, we equally treated all vessels in the OsSVM model. While this strategy helps avoid model overfitting, in surgical resection, the importance of surrounding vessels varies. For instance, it is more dangerous to damage celiac axis than other small veins. In future studies, we will prioritize the vessels according to their importance based on a larger patient sample.

5 Conclusion

In this study, we introduced a novel OsSVM method to quantify PC resectability based on contrast CT. We derived metrics that successfully classified LA, BR, and RE with high classification capacity. To the best of our knowledge, this is the first study to provide a quantitative definition of pancreatic tumor-vessel involvement by measuring the anatomical relationship of the two image objects. The proposed classifiers may provide an improved quantitative imaging guideline to refine the PC resectability grading system.

Acknowledgments

This research did not receive any specific grant from funding agencies in the public, commercial, or not-for-profit sectors.

References

[1]. Hidalgo M Pancreatic cancer. New England Journal of Medicine 362, 1605–1617 (2010). [PubMed: 20427809]

[2]. Howlader N et al. Anonymous surveillance epidemiology and end results of the national cancer institute. SEER Cancer Statistics Re- view: 1975–2014 Based on November 2016 SEER data submission, posted to the SEER web site, 4 2017.

[3]. Wong JC & Raman S Surgical resectability of pancreatic adenocarcinoma: Cta. Abdominal imaging 35, 471–480 (2010). [PubMed: 19468791]

[4]. Callery MP et al. Pretreatment assessment of resectable and borderline resectable pancreatic cancer: expert consensus statement. Annals of surgical oncology 16, 1727–1733 (2009). [PubMed: 19396496]

[5]. Gilbert J et al. Borderline resectable pancreatic cancer: conceptual evolution and current approach to image-based classification. Annals of Oncology 28, 2067–2076 (2017). [PubMed: 28407088]

[6]. Katz MH et al. Borderline resectable pancreatic cancer: need for standardization and methods for optimal clinical trial design. Annals of surgical oncology 20, 2787–2795 (2013). [PubMed: 23435609]

[7]. Morgan DE et al. Resectability of pancre- atic adenocarcinoma in patients with locally advanced disease downstaged by preoperative therapy: a challenge for mdct. American journal of roentgenology 194, 615–622 (2010). [PubMed: 20173136]

[8]. Hong SB et al. Pancreatic cancer CT: prediction of resectability according to NCCN criteria. Radiology 289, no. 3: 710–718 (2018).

[9]. Cristianini N, Shawe-Taylor J et al. An introduction to support vector machines and other kernel-based learning methods (Cambridge university press, 2000).

[10]. Shawe-Taylor J, Cristianini N et al. Ker- nel methods for pattern analysis (Cambridge university press, 2004).

[11]. Yip SS & Aerts HJ Applications and limitations of radiomics. Physics in Medicine & Biology 61, R150(2016). [PubMed: 27269645]

[12]. Yue Y et al. Identifying prognostic intratumor heterogeneity using pre- and post-radiotherapy 18f-FDG PET images for pancreatic cancer patients. Journal of gastrointestinal oncology 8, 127(2017). [PubMed: 28280617]

[13]. Eilaghi A et al. CT texture features are associated with overall survival in pancreatic ductal adenocarcinoma-a quantitative analysis. BMC medical imaging 17, 38(2017). [PubMed: 28629416]

[14]. Friedman J, Hastie T, & Tibshirani R Regularization paths for generalized linear models via coordinate descent. Journal of statistical software 33:1, 1 (2010). [PubMed: 20808728]

[15]. Matsakis P Understanding the spatial organization of image regions by means of force histograms: a guided tour. In Applying soft computing in defining spatial relations, 99–122 (Springer, 2002).

[16]. Ni J & Matsakis P Force histograms computed in o (nlogn). In Pattern Recognition, 2008. ICPR 2008. 19th International Conference on, 1–4 (IEEE, 2008).

[17]. Bloch I Fuzzy spatialrelationships for image processing and interpretation: a review. Image and Vision Computing 23, 89–110 (2005).

[18]. Hudelot C, Atif J & Bloch I Fuzzy spatial relation ontology for image interpreta- tion. Fuzzy Sets and Systems 159, 1929–1951 (2008).

[19]. Clément M, Poulenard A, Kurtz C & Wendling L Directional enlacement histograms for the description of complex spatial configurations between objects. IEEE transactions on pattern analysis and machine intelligence 39, 2366–2380 (2017). [PubMed: 28026752]

[20]. Toesca DA, et al., Predicting Pancreatic Cancer Resectability and Outcomes Based on an Objective Quantitative Scoring System. Pancreas, 48(5), 622(2019). [PubMed: 31091207]

[21]. Van Der Putten J et al. Quantitative ct based radiomics as predictor of resectability of pancreatic adenocarcinoma In Medical Imaging 2018: Computer-Aided Diagnosis, vol. 10575, 105753O(International Society for Optics and Photonics, 2018).

[22]. Vallières M et al. Responsible radiomics research for faster clinical translation (2018).

[23]. Rudyanto RD et al. Comparing algo- rithms for automated vessel segmentation in computed tomography scans of the lung: the vessel12 study. Medical image analysis 18, 1217–1232 (2014). [PubMed: 25113321]

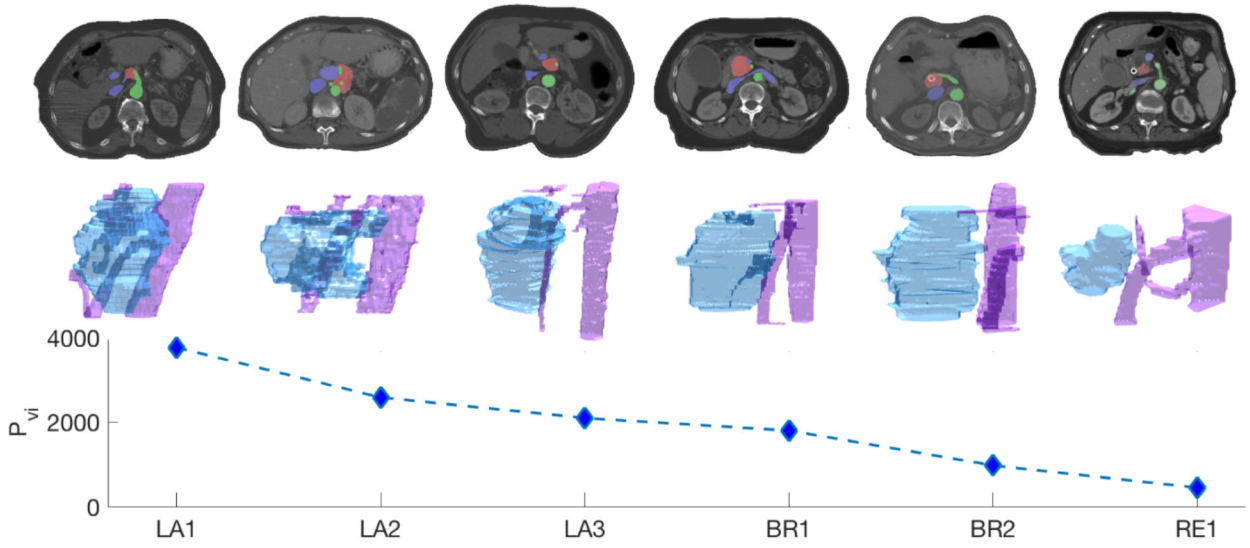

Figure 1:

Examples of patients with varying degrees of resectability and their corresponding resectability quantifications P_{vi}. The upper and middle rows show the axial views of the tumor vessel relationship (tumor, artery, and vein are marked in red, green and blue, respectively) and the corresponding 3D renderings of tumor (transparent blue) and vessels (transparent pink). The inter-subject differences spanning the wide spectrum from LA to RE had been quantitatively interpreted by Pvi shown in the bottom row. Note: the main vascular involvement presented in these subjects are arteries, thus veins were excluded in the 3D shape representation to yield better visualizations.

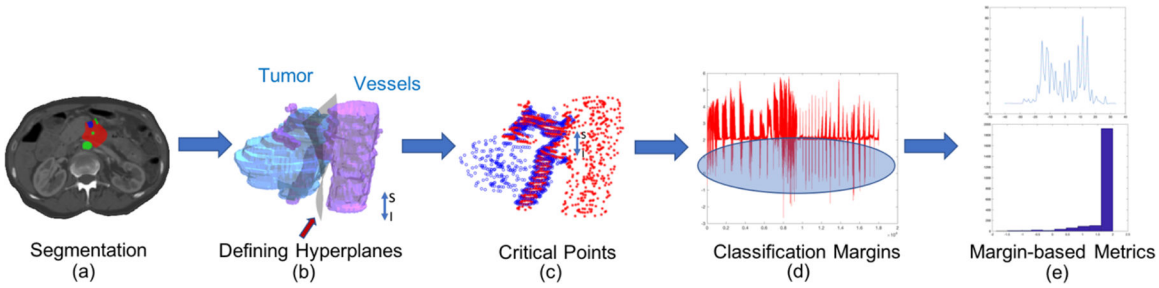

Figure 2:

Illustration of the pipeline quantifying vascular invasion using nonlinear OsSVM. (a) On contrast-CT images, the tumor and vessels are manually segmented and processed to create the intra-subject VOI. Tumor, artery, and vein are color-coded by red, green and blue, respectively. (b) A hyperplane is defined in VOI using OsSVM. (c) Support vectors from OsSVM are selected as critical points fed into the following analysis. (d) Classification confidence measurements (margins) are calculated for the critical points corresponding to the class *vessel* and used as indicators of vascular invasion. Points with margin value located in the blue area correspond to points with low classification confidence (critical points). (e) Metrics are developed based on the spatial distribution of margins (upper) and margin-histograms (bottom).

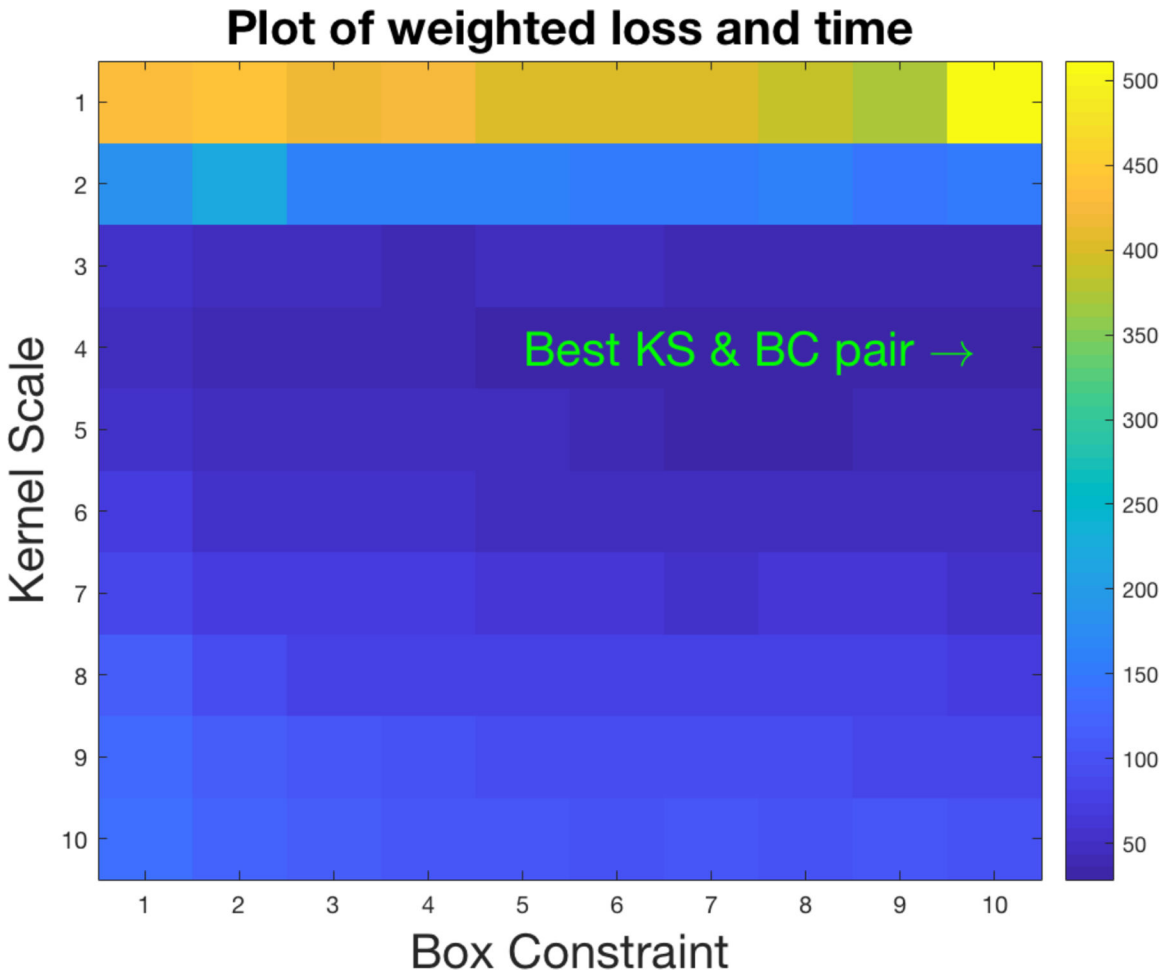

Figure 3:

Illustration of the selection criteria of hyperparameters kernel scale (γ) and box constraint (C). A combination of $\gamma = 4$ and $C = 10$ resulted in a minimal of weighted R0 classification loss (misclassification rate) and runtime (s).

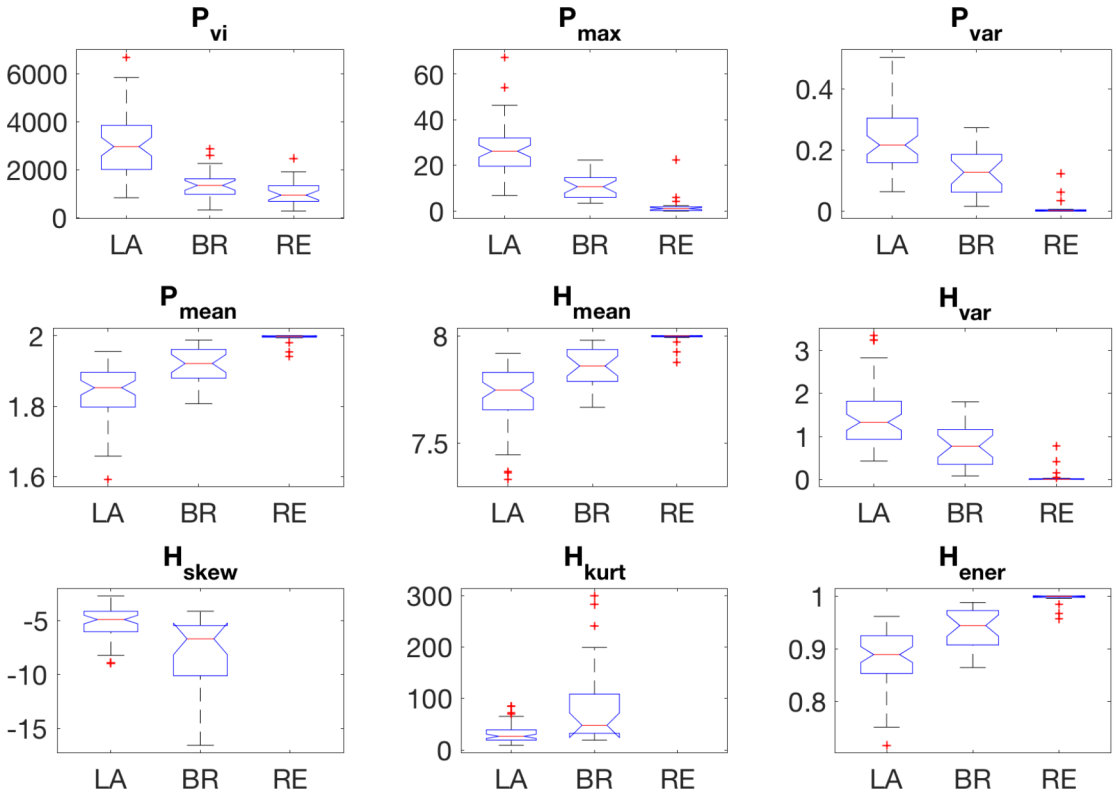

Figure 4:

Box plots revealing the distribution of 9 features in groups with varying degrees of resectability: LA, BR, and RE.

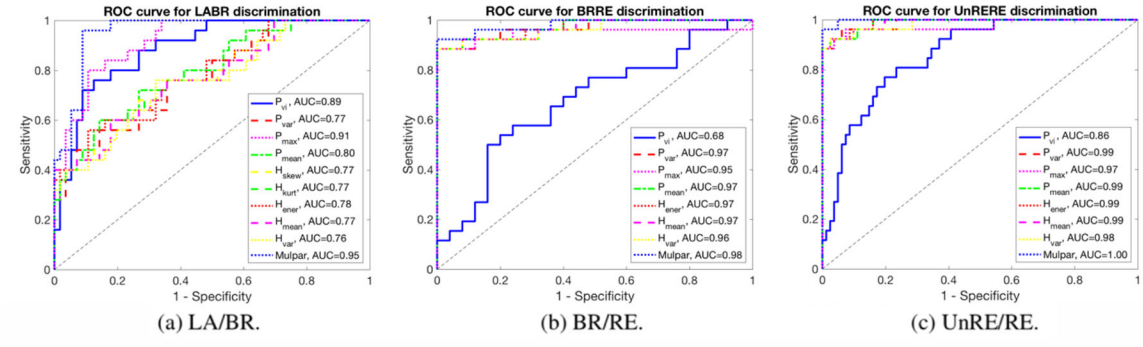

Figure 5:

ROC curves for the discrimination of LA and BR (a), BR and RE (b), as well as UnRE (LA + BR) and RE (c).

Table 1:

Summary of statistical group comparison results.

	LA		*BR*		*RE*		*LA/BRP*	*BR/REP*	*UnRE/REP*
	Mean	***Std***	**Mean**	***Std***	**Mean**	***Std***			
P_{vi}	3000.3	1256.0	1384.1	630.0	1047.7	548.0	<0.0001	0.0471	<0.0001
P_{var}	0.2	0.1	0.1	0.1	0.0	0.0	<0.0001	<0.0001	<0.0001
P_{max}	27.5	11.6	11.2	5.8	2.1	4.4	<0.0001	<0.0001	<0.0001
P_{mean}	1.8	0.1	1.9	0.1	2.0	0.0	<0.0001	<0.0001	<0.0001
H_{skew} [1]	−5.2	1.5	−8.3	3.9	-	-	<0.0001	-	-
H_{kurt} [1]	32.1	18.3	89.7	84.5	-	-	<0.0001	-	-
H_{ener}	0.9	0.1	0.9	0.0	10.5	0.0	<0.0001	<0.0001	<0.0001
H_{mean}	7.7	0.1	7.9	0.1	27.6	0.0	0.0001	<0.0001	<0.0001
H_{var}	1.4	0.7	0.8	0.6	169.3	0.2	0.0001	<0.0001	<0.0001

[1] Due to the missing bins in RE cases, Hskew and Hkurt were excluded from RE related calculations.

Table 2:

Summary of univariate and multivariate (EN) regression results for the discrimination of LA vs. BR, BR vs. RE, as well as UnRE vs. RE.

	LA vs. BR			*BR vs. RE*			*UnRE vs. RE*		
	β_u [1]	p_u [1]	β_{EN} [2]	β_u	p_u	β_{EN}	β_u	p_u	β_{EN}
P_{vi}	−12.73	<0.0001	−3.34	−2.62	0.0558	-	−12.02	<0.0001	−0.35
P_{var}	−6.27	0.0003	-	−13.86	0.0008	−0.56	−29.16	<0.0001	−2.29
P_{max}	−15.66	<0.0001	−3.18	−9.15	0.0005	−0.85	−30.78	<0.0001	−3.03
P_{mean}	8.10	0.0002	0.64	18.27	0.0006	1.19	42.05	<0.0001	2.74
H_{skew} [3]	−7.01	0.0004	−1.10	-	-	-	-	-	-
H_{kurt} [3]	9.98	0.0018	1.01	-	-	-	-	-	-
H_{ener}	7.06	0.0003	-	17.96	0.0008	1.00	40.42	0.0001	3.74
H_{mean}	6.47	0.0006	-	15.81	0.0010	-	35.94	<0.0001	-
H_{var}	−5.88	0.0007	-	−13.69	0.0011	-	−29.89	<0.0001	−0.12

[1] Regression coefficients and p-values obtained from univariate logistic regression.

[2] Regression coefficients for metrics selected from the elastic net (EN).

[3] Due to the missing bins in RE cases, Hskew and Hkurt were excluded from RE related calculations.